Combined 3D model acquisition and autofocus tracking system for hyperspectral line-scanning devices

Asgeir Bjorgan, Lukasz A. Paluchowski, Svein Tore Koksrud Seljebotn and Lise Lyngsnes Randeberg

Department of Electronic Systems, NTNU Norwegian University of Science and Technology, Trondheim, Norway

ABSTRACT

Obtaining a sharp and focused image is essential to fully utilize the advantages of hyperspectral imaging. For line scanning hyperspectral devices, focusing is a challenge in applications where the height and/or position of the imaged object might vary during a scan. Initial focusing is in addition a tedious process that has to be repeated for each sample or measurement. In this paper, a new continuous autofocus tracking system for hyperspectral line-scanning cameras is reported. The presented system is able to automatically and objectively find the correct distance between the camera and the imaged object for proper focus, and retain this focus distance during scan using a laser triangulation system. Concurrent with the focusing, a 3D model of the object is constructed. The system was tested and found to perform well for NIR-SWIR imaging of human hands and test objects with sharp changes in height and contrast. The method is easily adaptable to other spectral ranges and applications, such as industrial conveyor belt applications. The method significantly eases the acquisition of hyperspectral images by ensuring optimal image quality in every scan and eliminating the need for manual refocusing between individual samples.

Keywords: image quality, spectroscopy, biomedical imaging, digital elevation models, automatic control, push-broom

1. INTRODUCTION

Hyperspectral imaging is a non-contact imaging technique that provides both spatial and spectral information in one modality. This spectroscopic information can be valuable for a wide range of applications like remote sensing, food quality control, waste sorting and medical imaging.[1–9] Ensuring good focus of the camera is crucial in achieving the image quality necessary for a given application. This becomes more challenging with increasing image resolution, since the depth of field of the lens decreases and minimizes the acceptable deviations in the focus distance to the imaged object.

Camera aberrations become more evident and the images will be blurred when the camera is out of focus. Blurring reduces the available detail and contrast in the image, degrading the image quality. Deviations from the correct focus distance can result in variations in amplitude due to variation in light intensity. This propagates into errors in the analysis for applications which require strict illumination control.

An example from imaging of human skin is shown in Fig. 1. The spectral differences shown here will lead to systematic deviations in the spectral analysis. It is expected that these deviations will vary as the object goes in and out of focus, and lead to inaccurate recording of the spectra collected from a sample. Blurring such as shown in Fig. 1 can be a hindrance to spatial analysis by obscuring smaller details like wound boundaries, moles or blood vessels.

Non-flat objects intensifies these challenges. Focusing the camera on one part of the object requires refocusing throughout the scan. For hyperspectral imaging of living humans, this causes unneccessary stress to both the patient and the operator if done manually. Imaging of objects of various sizes on a conveyor belt has similar challenges. It is therefore a need for a general method for adjusting the hyperspectral focus automatically throughout a scan. This method should guarantee optimal focus quality and provide the objective means to evaluate any deviations.

Further author information: (Send correspondence to A.B.)
A.B.: E-mail: asgeir.bjorgan@ntnu.no

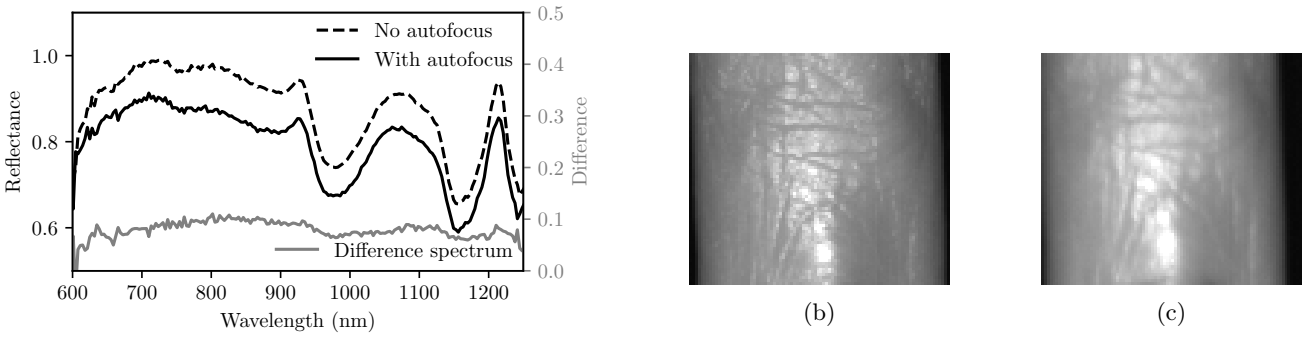

(a) (b) (c)

Figure 1: Hyperspectral reflectance spectra (a) and band images at 1210 nm acquired from a human finger with (b) and without (c) the autofocus solution presented in this paper.

Focusing techniques are commonly grouped into active and passive autofocusing techniques. Passive autofocusing techniques rely on in-camera information after the light has passed through the lens. Phase detection and contrast measurement[10] are two common ways to do this. Phase detection can quickly yield information on how the lens should be moved, but requires fragile and expensive components as well as careful calibration. Contrast measurement works directly on the hyperspectral image without extra equipment, but can yield only relative measures of the contrast quality and will not give any information on direction of lens movement. Passive methods are also susceptible to the illumination conditions.

Active autofocusing relies on information outside the camera by actively transmitting energy to the environment and sensing the environment response. Examples include using ultrasound, laser light or infrared light to calculate the distance to the imaged object. The technique requires extra equipment, but can in many cases be done inexpensively. Such techniques can be used regardless of the light conditions on the scene and without changing the optics. Only one solution for autofocusing in hyperspectral imaging of paintings was found in the literature.[11] Some methods are available for focusing in hyperspectral microscopy.[12]

The solution presented in this paper is two-fold: The optimal focus distance between the camera and the object is determined using a passive contrast measurement technique by scanning in the vertical direction. Focus distance between the camera and a topographically varying object is maintained during the scan by actively measuring height changes in advance and progressively adjusting the height of the translation stage. A full 3D profile is acquired along-track, enabling both 3D modeling of the hyperspectral image for corrections in illumination and more advanced selection of focus points.

The primary application for the system presented here is the NIR-SWIR imaging of human hands, but it can be used for a wide range of applications. The developed system is simple, requires few components and relies on in-camera information to objectively evaluate the focus quality. The system can augment any hyperspectral lab setup with the ability to obtain measurements with optimal image quality and a stable spectral response.

The paper is organized in five sections: In section 2, implementation of the tracking solution is detailed. Section 3 presents the calibration of the system parameters, including the objective method for automatically estimating the focus distance. Sections 4 and 5 present the experimental tests done to evaluate the performance of the system.

2. SYSTEM IMPLEMENTATION

2.1 Hyperspectral system

The system consists of a custom-made hyperspectral push-broom camera developed by Norsk Elektro Optikk (Skedsmokorset, Norway) mounted on a horizontal motorized translation stage with 20 cm translation range (8SMC4-USB-B8-1 (controller), 8MT50-200BS1 (stage), Standa, Vilnius, Lithuania). The hyperspectral camera records one image line (640 pixels) at a time with a adjustable speed of 5-90 ms per line of data. The working distance of the hyperspectral camera is 30 cm and the field of view (FOV) is 12.0 cm with the optics used in this

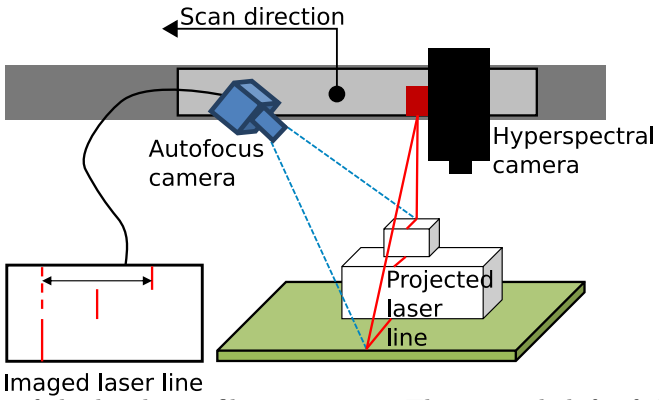

Figure 2: Working principle of the height profile acquisition. The vertical shift of the laser line is captured by the autofocus camera and translated to a height profile by the software.

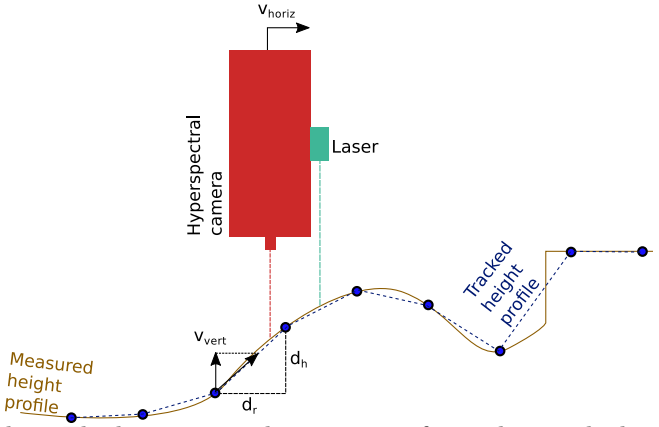

Figure 3: Refocusing algorithm. The hyperspectral camera is refocused towards discrete refocusing points along the measured height profile.

setup. The depth of field of the lens was 0.5 cm. The spectral range covered by the camera is 600 - 1200 nm, with a spectral resolution of 3.4 nm across 170 bands. The scene is illuminated with two light sources (3900e, Illumination Technologies, East Syracuse, NY, USA) attached to the camera, providing spatially uniform light across the FOV.

2.2 Autofocus system

The autofocus system acquires height profiles at a distance Δs_{laser} in front of the current hyperspectral FOV. The horizontal translation stage is used to scan over the imaged object using a speed v_{horiz} (steps/s), given by the chosen frame period of the hyperspectral camera. Hyperspectral lines and height profiles are collected to a full hyperspectral image and 3D model, respectively. The height profiles are used to automatically adjust the height of the hyperspectral camera in real-time, in such a way that the entire image remains in focus during the scanning process.

2.2.1 Hardware configuration

The hardware configuration of the autofocus setup is shown in Fig. 2. In order to adjust the working distance, the hyperspectral camera is mounted on a vertical motorized translation stage (8SMC4-USB-B9-2 (controller), 8MVT100-25-1 (stage), Standa, Vilnius, Lithuania). A self-developed laser triangulation system is used to record object topography. A green line laser (Z-LASER Z5M18B-F-532-LG30-V2, Stemmer Imaging AB, Stockholm, Sweden) is used to project a laser plane at 532 nm. The laser line is recorded by a monochromatic video camera (DCC1240M, ThorLabs, Newton, New Jersey, USA). A narrow band pass filter (ThorLabs, Newton, New Jersey, USA) with center wavelength corresponding to the spectral range of the laser is mounted on the lens to reduce ambient light.

The line laser is rigidly fixed to the hyperspectral camera and projects the laser plane parallel to the FOV of the hyperspectral camera, approximately 4.5 cm in front of the FOV. The video camera is fixed only to the horizontal translation stage, and not the vertical translation stage. This ensures that the recorded position of the imaged laser line depends only on the height of the object at the laser line position, and not on the translatable vertical camera position.

2.2.2 Height acquisition

The height acquisition system was specially designed for the purpose of continuous autofocus for a hyperspectral line scanner. Retaining focus requires only relative changes of object height from a known focus distance. The height of the imaged object is therefore always measured from a calibrated reference plane, where the vertical translation stage position for the sharpest focus of the hyperspectral camera is known.

Any object placed above or below the reference plane causes a deviation from the necessary focus distance, and a corresponding displacement of the laser line from its initial position as viewed by the monochromatic camera. The shift of the laser line on the image is then used to calculate the object height.

The height profiles are extracted from a live video stream from the monochromatic camera using simple image processing algorithms. The laser line is captured as a bright line across the column-direction of the image frame, and shifts in the laser line lead to changes in the position along the row direction of the frame. Each video frame is thresholded and median filtered in order to remove background and reduce speckle noise. The thresholded profile is reduced to a 1 pixel thick centerline of each connected component in the row-direction, and the height profile $h_{p,raw}(j)$ in terms of pixels is set to the row-position of the first encountered non-zero pixel from the bottom of the video frame. The variable j corresponds to the column coordinate along the FOV of the autofocus camera.

The raw height profile $h_{p,raw}(j)$ is translated to a calibrated height $s(j)$ in terms of steps along the translation stage using

$$s(j) = (h_{p,raw}(j) - h_{p,ref}(j))\frac{\Delta s}{\Delta h_p} + s_{ref}. \tag{1}$$

The acquired height profile of the reference plane is denoted by $h_{p,ref}(j)$. The corresponding optimal focus position for the hyperspectral camera at the reference plane is s_{ref}. The number of vertical steps per pixel shift in the monochromatic frame is $\frac{\Delta s}{\Delta h_p}$. The calibration of these three parameters are further described in section 3. The height profile $s(j)$ describes the translation step at which the hyperspectral camera has the across-track position j in focus.

Each laser profile is coupled to the current horizontal translation stage position s_{horiz} at the time of acquisition, yielding a model $s_{vert}(j, s_{horiz} + \Delta s_{laser})$. The model can be translated to physical units using the number of length units per vertical translation step $\frac{\Delta h}{\Delta s}$. This yields a complete 3D model of the imaged object. However, for camera height adjustments, a single height is needed along-track. It is desired that the height selection keeps as much as possible of the FOV of the imaged object in focus. Two simple solutions were proposed for this study:

- Select the translation stage position $s(j)$ corresponding to a fixed $j = j_0$ in the center of FOV.
- Select the translation stage position $s(j)$ corresponding to the maximum $s(j)$ across the center of FOV.

The primary application of the system presented in this study is the imaging of human hands. Selecting a fixed position can potentially cause the system to track heights placed exactly in the middle of two fingers. Selecting the maximum height ensures that one of the fingers always remain in focus, while the focus on the rest of the fingers is dependent on the depth of field of the lens in use. The deviation can be evaluated using the 3D model. The strategy of always choosing the maximum height is also suitable for other imaged objects.

2.2.3 Continuous height adjustments during scan

The object topography is available for a given length in front of the FOV of the hyperspectral camera, enabling the working distance to be adjusted in advance of changes in height. Possible height adjustment methods include a feed-forward PID (proportional–integral–derivative) regulator, adjustment of speed and acceleration to approximate the height profile in curve segments, or adjustment of speed to approximate the profile in line segments.

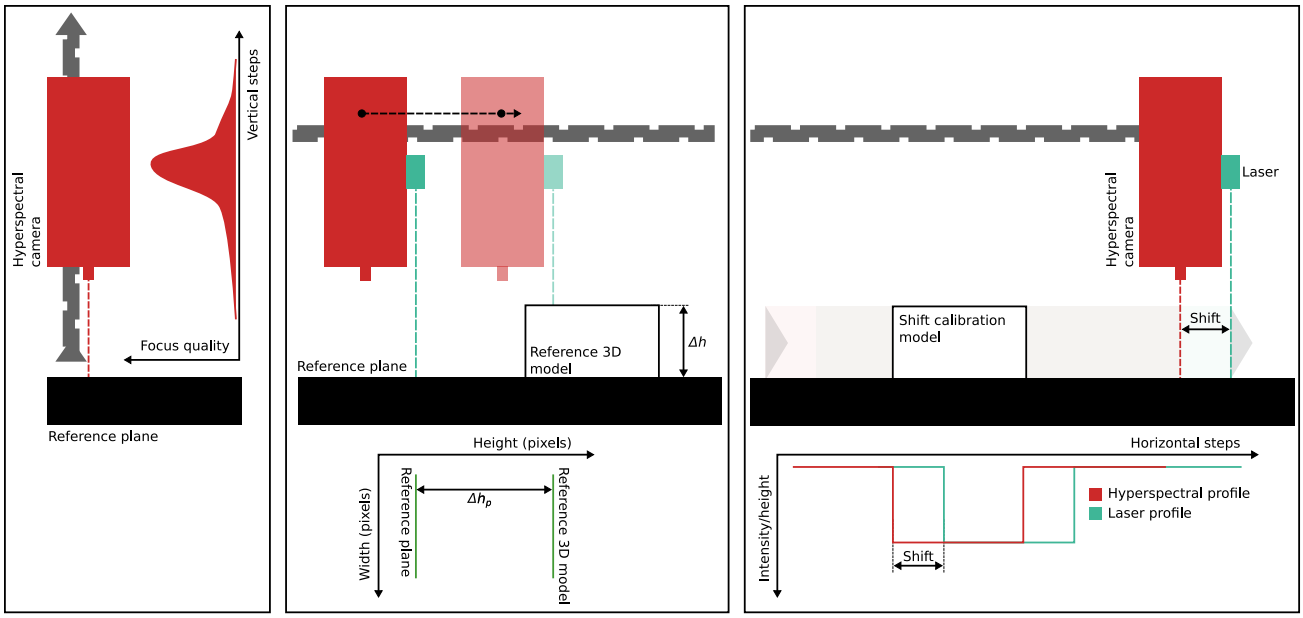

Figure 4: Calibration of the autofocus system: (a) initial focus, (b) vertical translation steps per pixel shift and (c) shift between FOV and the laser line.

For the current study, the latter method was used, due to its simplicity and robustness. The method is illustrated in Fig. 3. This strategy is suitable mainly for smoothly varying objects due to its tendency to skip over sharp changes in height. At a given refocusing point i, a new speed and position are issued to the vertical translation stage in order for it to reach the given height at the next refocusing point $i+1$. At the current refocusing position $s_{horiz}(i)$, the object height $s_{vert}(i+1)$ at the next refocusing position $s_{horiz}(i+1)$ is obtained from the acquired height profiles, yielding the differences $\Delta d_v = s_{vert}(i+1) - s_{vert}(i)$ and $\Delta d_h = s_{horiz}(i+1) - s_{horiz}(i)$. Using the horizontal scanning speed v_{horiz} of the horizontal translation stage and assuming instantaneous acceleration and deacceleration, the necessary vertical translation speed can be calculated using

$$v_{vert} = \frac{\Delta d_v}{\Delta d_h} v_{horiz}. \tag{2}$$

The measured along-track height profile is smoothed using central moving average (CMA) in order to avoid noise and subsequent unnecessary and deviating movement of the camera.

3. SYSTEM CALIBRATION

The system characteristics necessary for focusing are the laser-FOV distance Δs_{laser}, the acquired height profile of the reference plane $h_{p,ref}(j)$, its corresponding optimal focus position s_{ref} and the number of steps per pixel shift $\frac{\Delta s}{\Delta h_p}$. The calibration of each of these are described below and in Fig. 4.

3.1 Acquisition of reference plane and initial focus position

Relative height changes are measured from a fixed height profile acquired from a reference plane. The reference plane is coupled to a known vertical position where the distance between the reference plane and the hyperspectral camera corresponds to the focus distance.

The optimal focus distance is found by measuring the focus as a function of the vertical hyperspectral camera position on e.g. a checkerboard pattern. Focus is in this case measured by quantifying the contrast in each hyperspectral line of data. Suitable measures of contrast include gray level variance, energy of gradient, energy of second derivative, histogram entropy and the discrete wavelet transform[10,13,14].[15] The type of imaged object, light conditions and the camera sensor influences which algorithm yields the best result in a given situation.[13]

Additionally, the hyperspectral image must be reduced to a monochromatic image before being fed to a given focus algorithm. The visibility of the object across different wavelengths and the SNR of the hyperspectral sensor response influences which bands should be chosen. Using the luminance from a YCbCr conversion can be suitable for cameras operating in the visible range.[14] The camera in this study is well outside the range where YCbCr is well-defined, and a different approach was used.

A checkerboard pattern was printed on white paper using a standard laser printer. The checkerboard pattern was found to have high contrast up to 860 nm and from 1300 nm and up. Additionally, the hyperspectral camera was designed to have maximum SNR at 1080 nm. Band images were selected from each wavelength region and combined using the arithmetic mean. The previously mentioned algorithms were tested as a part of a previous study, and the energy of gradient was in particular found to perform well for both low-contrast and high-contrast objects under low- and high-SNR conditions. As the energy of gradient was found to be applicable in characterizing the focus distance also in this case, this algorithm was not extensively compared against other alternatives for this specific problem.

The system used in this study is a black-box system built for one purpose, where all components are rigidly fixed. The initial focus procedure can in this case be done infrequently. As a part of a more general, flexible system, it can be necessary to run an initial focus procedure at the start of each scan. It can also be desirable to always rerun the initial focus procedure on a reference plane placed in the center of the expected height range, in order to minimize the effect of potential systematic deviations due to inaccurate calibration or system drift.

3.2 Shift between laser plane and hyperspectral FOV

The shift between the hyperspectral FOV and the laser FOV is calibrated by scanning over a flat, square object with a high contrast against the background. Using the horizontal translation speed, the hyperspectral frame period and assuming minimal lag between the start of hyperspectral scan and the start of the translating motion, the line number of the hyperspectral camera is coupled to horizontal steps along the image. The along-track laser-profile and hyperspectral profile of the square object will then show up as sharp changes in contrast/height with the same units along the scan direction. The shift between these can then be found using simple cross-correlation.

3.3 Number of steps per pixel shift

Height change in millimeters per pixel shift of the laser line ($\frac{\Delta h}{\Delta h_p}$) as viewed by the monochromatic camera is calibrated using a 3D model with known height Δh. Height profiles $h_{1,p,raw}(j)$ and $h_{2,p,raw}(j)$ are acquired on top of the 3D model and from the reference plane, respectively. The difference Δh_p is set to the mean shift between h_1 and h_2. The vertical translation stage's full translation range is measured both in terms of centimeters and number of translation steps, yielding the number of steps per centimeter $\frac{\Delta s}{\Delta h}$. Combining the two yields the number of steps per pixel shift, $\frac{\Delta s}{\Delta h_p}$. This also defines the minimum step size of the system.

4. EXPERIMENTAL EVALUATION SETUP

The chosen passive algorithm for calculating the focus was applied to a text pattern tilted 60 degrees. The correct focus distance was derived by scanning in the vertical direction. Scans were then run in either horizontal direction with the apparent focus height in order to confirm the gradual loss of focus.

The continuous active autofocus tracking system was tested on various objects in order to evaluate the tracking accuracy and the subsequent image quality:

- A pattern with 15 degrees tilt (flat, smooth increase in height).
- A human hand (smooth changes in height).
- Two staircases built in LEGO (steep changes in height and contrast, see Fig. 5).

The LEGO and hand images were evaluated through visual inspection, as the passive focus algorithm is too heavily dependent on along-track changes in contrast to give any reliable results for these types of object. An objective evaluation was possible on the tilted pattern due to the homogeneous appearance along-track the object. Here, energy of the second derivative was used as a measure of the contrast.

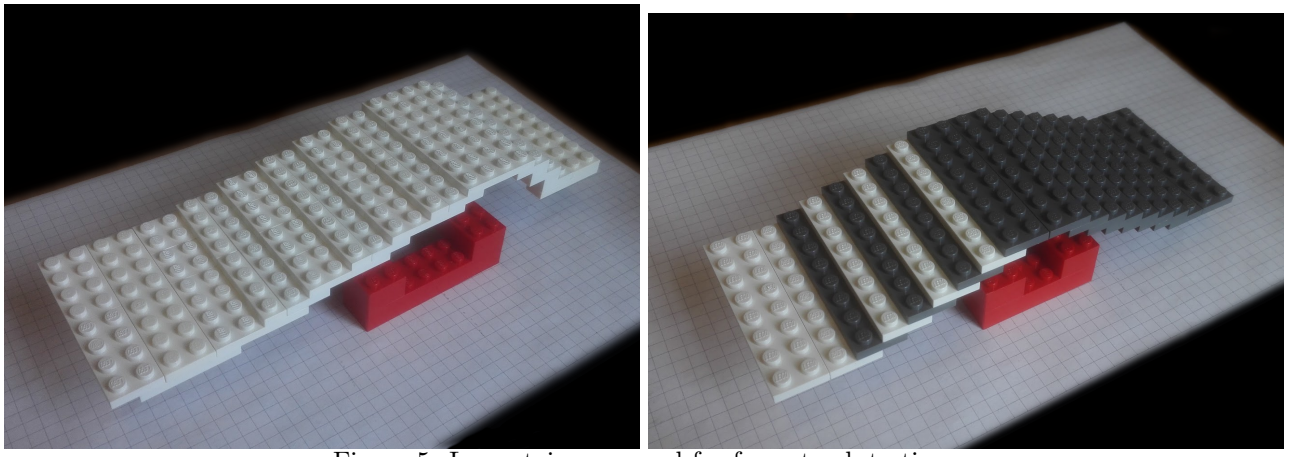

Figure 5: Lego staircases used for focus track testing.

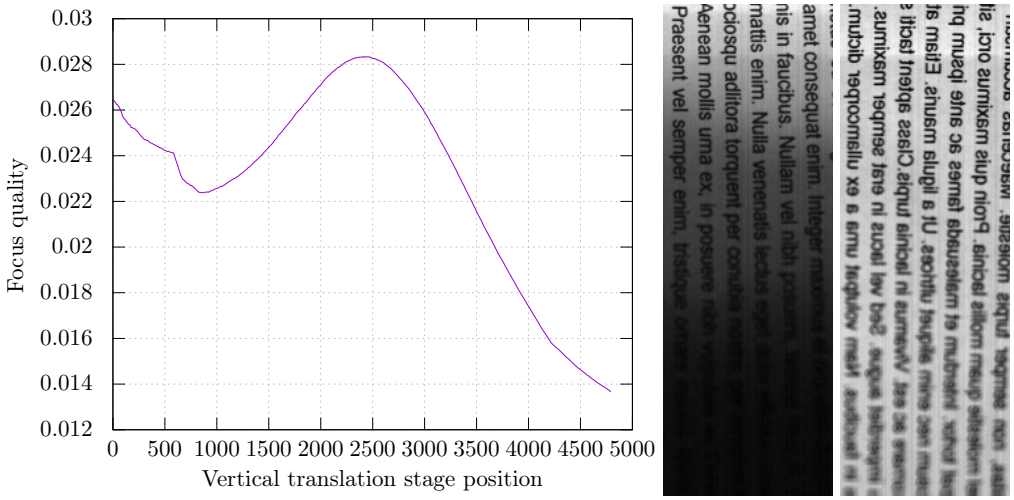

(a) (b) (c)

Figure 6: Initial focusing on a tilted text pattern: (a) Focus as a function of translation steps along the vertical translation stage, and scans (b) up and (c) down the tilted pattern from the initial position, with the camera fixed at the derived focus distance.

5. EXPERIMENTAL EVALUATION RESULTS AND DISCUSSION

The developed autofocus system was tested on a text pattern, a checkerboard pattern, a human hand and LEGO staircases in order to evaluate the focus quality.

5.1 Initial focus

Results from the passive initial focusing algorithm on a tilted checkerboard pattern is shown in Fig. 6. The line numbers with sharpest focus show up as a peak in the focus plot. Scans in either direction of the tilted text show a continued sharpness of the text, indicating a relatively large depth of field, until the focus is reduced. This confirms that the initial focus algorithm is able to automatically find the correct focus distance in terms of vertical translation steps.

5.2 Focus quality

5.2.1 Smooth changes in height

Profiles from both the tilted pattern (Fig. 7) and the human hand (Fig. 8) show that the system is able to track the measured height profile well, with low deviations. Though the tracked profile is close to the measured profile, the actual focus is dependent on the accuracy of the calibration parameters, and must be evaluated separately.

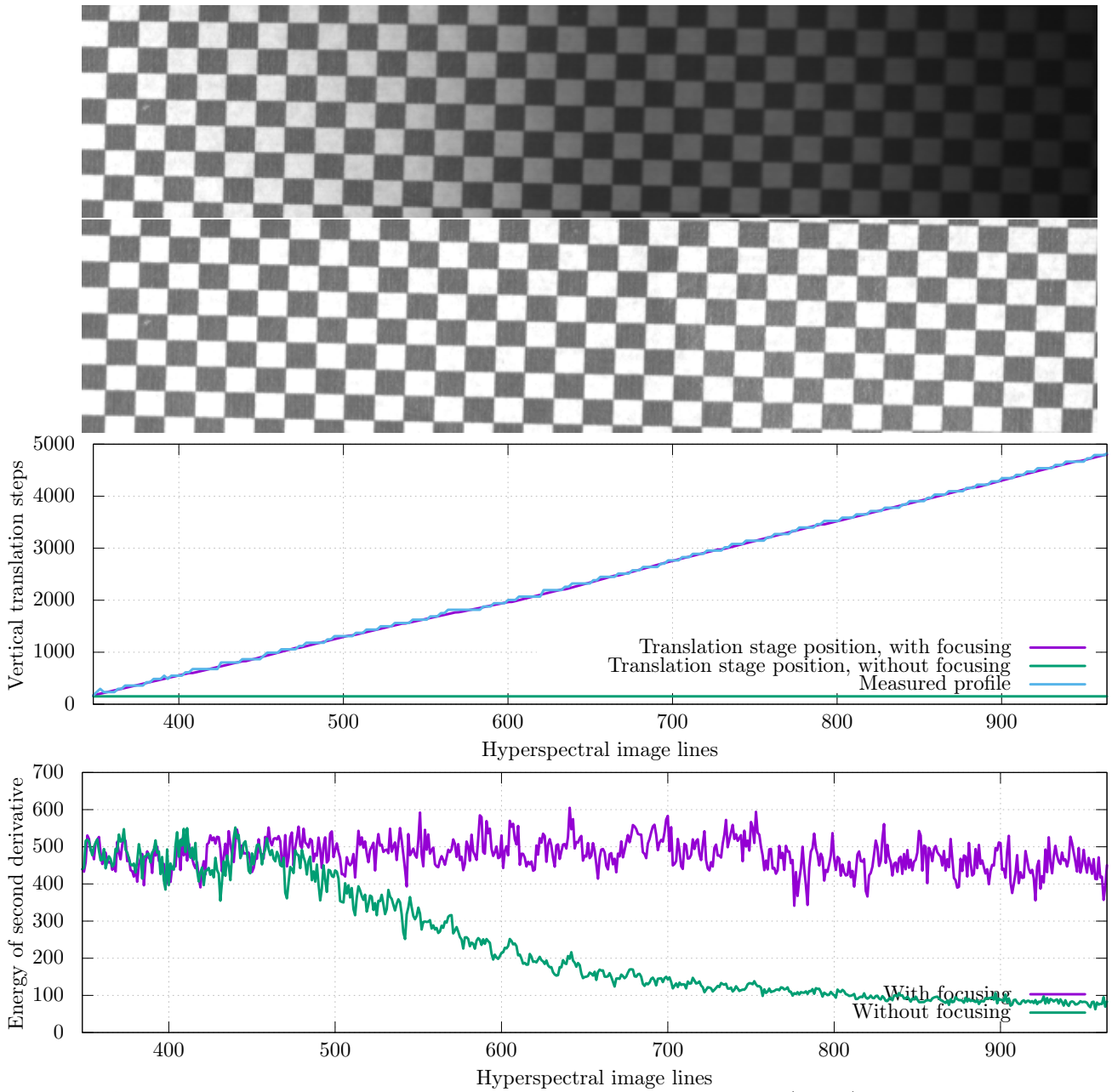

Figure 7: Autofocus tracking on a tilted pattern, without and with autofocus (above). Tracked profile and the calculated focus quality is shown below.

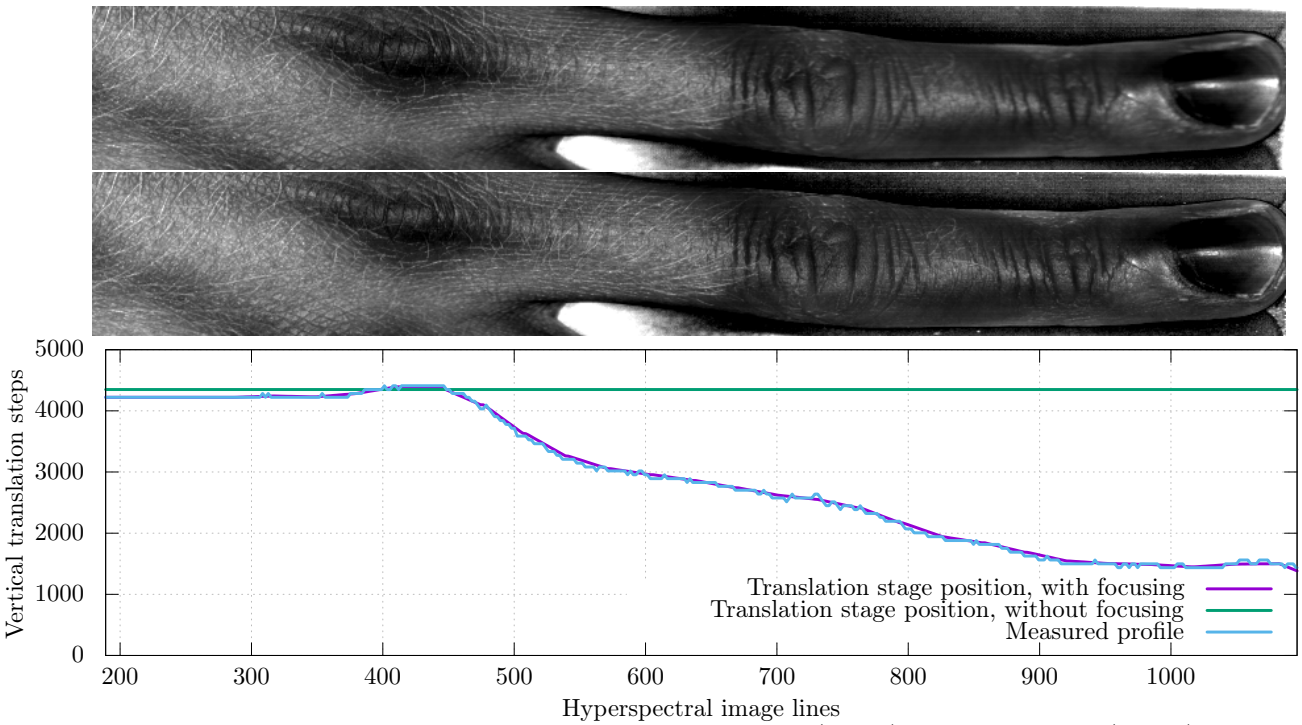

Figure 8: Autofocus tracking of a human hand, without autofocus (above), with autofocus (center) and the tracked height profile (below).

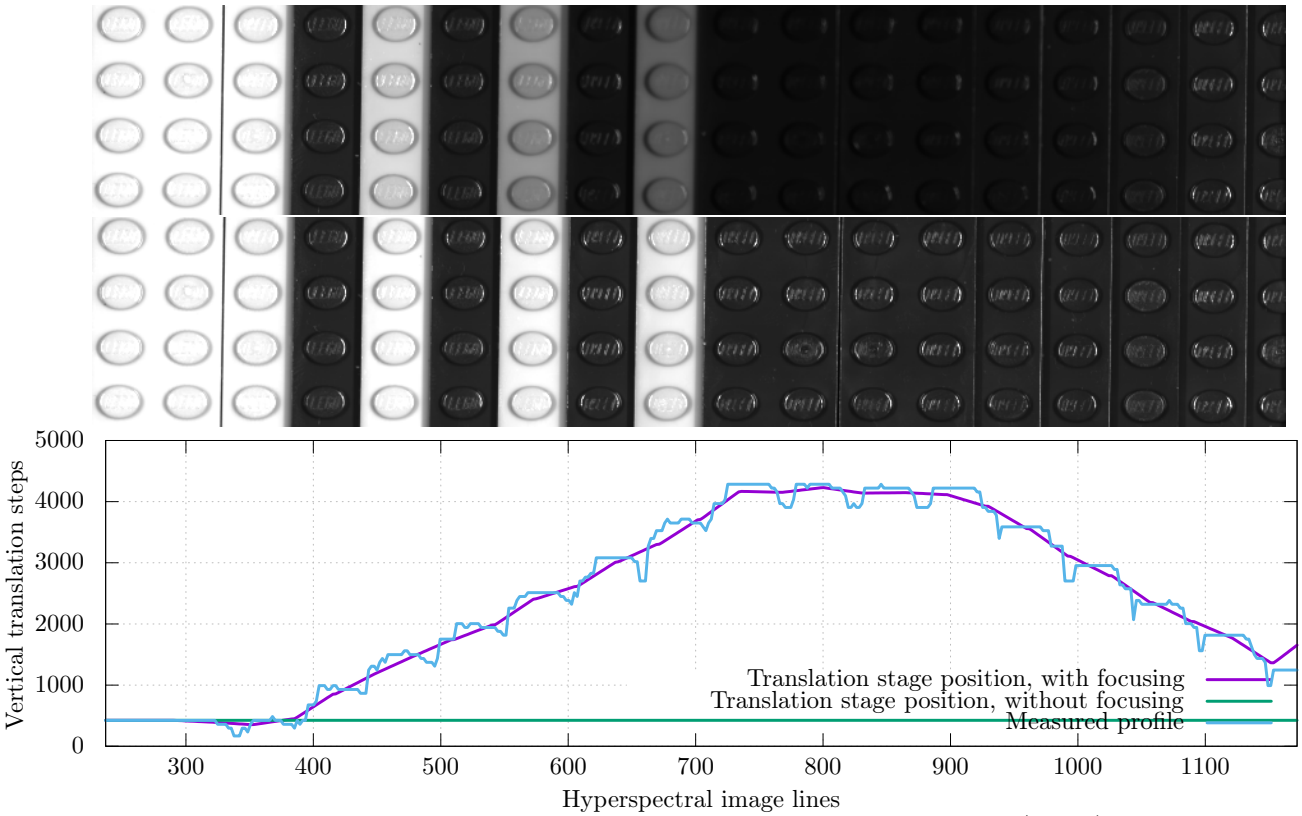

Figure 9: Autofocus tracking of white and grey LEGO staircase, without autofocus (above), with autofocus (center) and the tracked height profile (below).

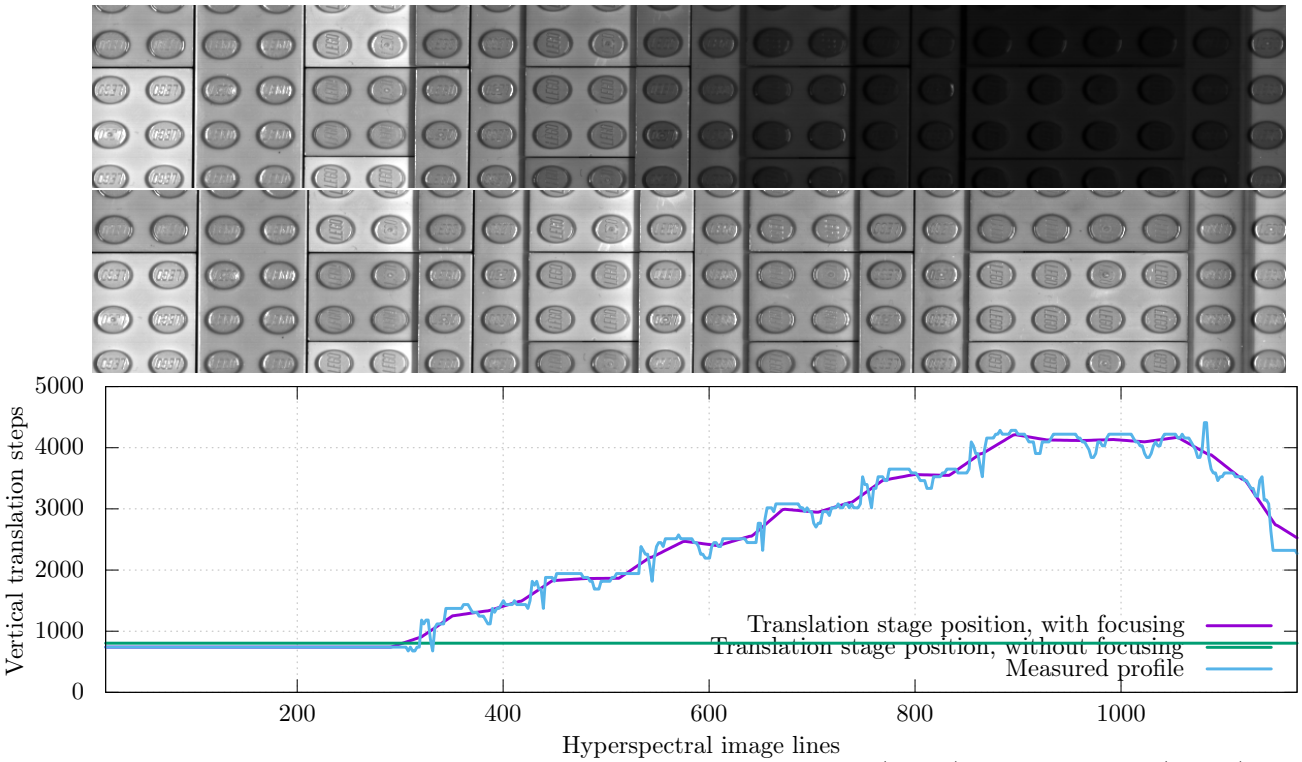

Figure 10: Autofocus tracking of white LEGO staircase, without autofocus (above), with autofocus (center) and the tracked height profile (below).

Comparing images with and without autofocus for one of the fingers, and judging by the finer details like hair and skin folds, it can be seen that the image collected with autofocus has better focus. The fifth digit of the hand was slightly out of focus, even though the central fingers showed good focus. This is explained by the strategy for choosing the across-track focus point, where the distance closest to the camera is always selected. This yields good focus for the center fingers, but fingers like e.g. the fifth digit will be just within or slightly out of the depth of field of the lens. Optimal focus for all fingers can be obtained by scanning multiple times and tracking each of the fingers during each scan. The tilted pattern is consistent across the image, indicating no major systematic deviations in the calibrated parameters.

The energy of the second derivative was calculated for the checkerboard pattern as a function of the along-track position (Fig. 7). As a contrast measure, it shows mostly stable behavior for the image tracked with autofocus. However, there are also some deviations after line 750. This is likely due to a slight tilt of the pattern across-track the image combined with the pattern not being perfectly aligned with the along-track direction, resulting in some illumination differences at this point and increased specular reflection. This is also seen in the image.

In addition to improved contrast quality, improved image quality and the ability to discern finer details, the autofocus tracking also provides even illumination throughout the image. This is best illustrated by comparing the tilted pattern with and without autofocus, as images without autofocus become darker and have non-uniform illumination. This is also, however, dependent on the distance across the field of view. As the imaged object falls out of focus across the FOV (like for a curved human hand), the illumination conditions also change. The autofocus system presented in this study provides a digital elevation model of the imaged object. When correctly coupled to the hyperspectral image, the model can be used for rectification of the illumination conditions. This coupling and the subsequent corrections will be implemented as a part of future work. Some profiles extracted from the 3D model of the human hand are shown in Fig. 11.

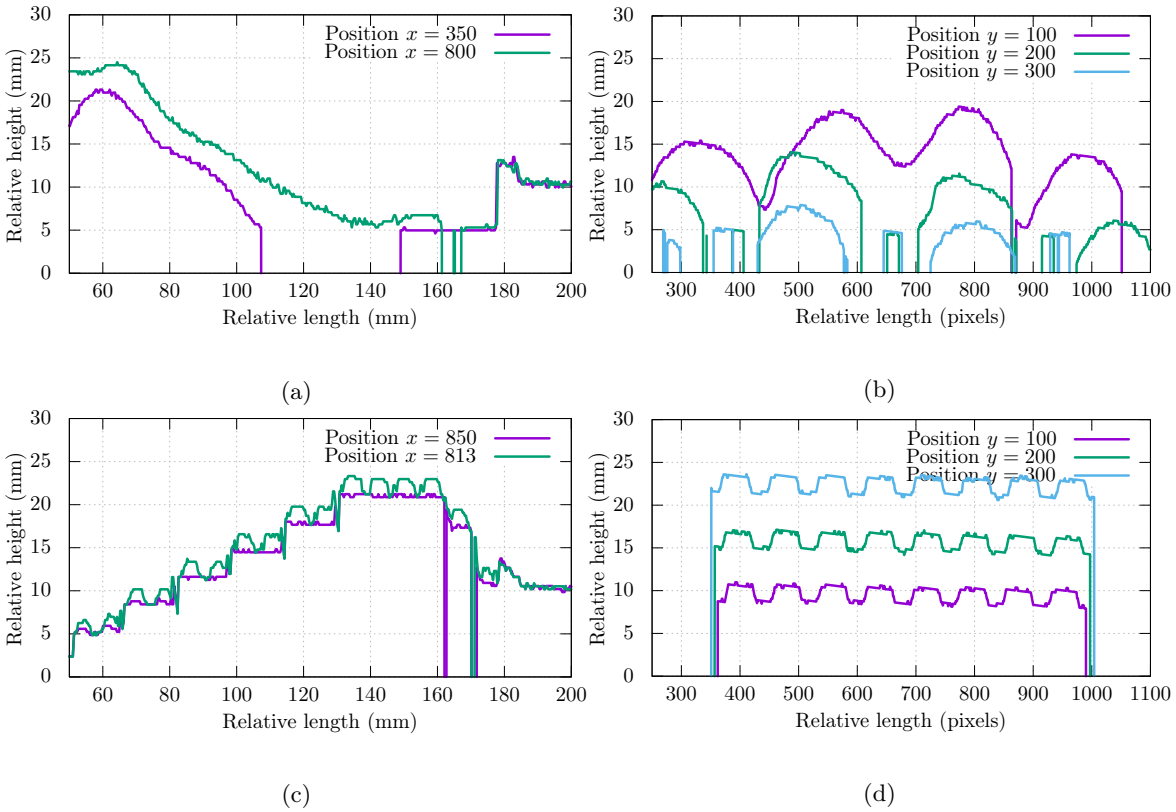

Figure 11: 3D model profiles: fingers along-track (a) and across-track (b), LEGO staircase along-track (c) and across-track (d).

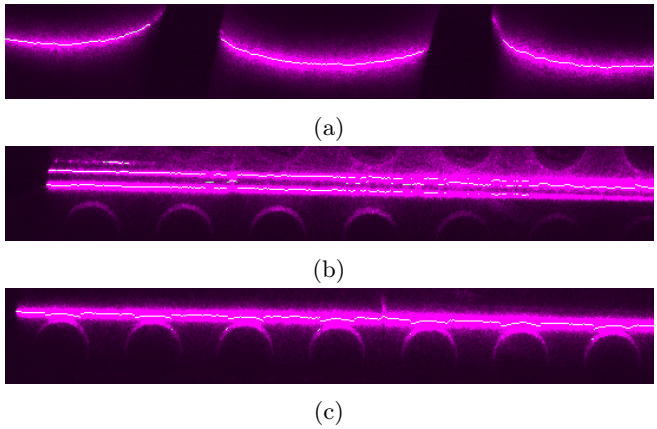

Figure 12: Autofocus profiles as viewed by the autofocus camera: fingers (a), LEGO with major vertical reflections (b), LEGO with minor reflections (c). Raw profiles are shown in purple, while the detected, processed centerline is shown in white.

5.2.2 Sharp changes in height

For biomedical applications of hyperspectral imaging, with gradual changes in height, the focusing strategy in this study yields reasonable results. The system's response to sharp changes in height (Figs. 9 and 10) is less accurate. Even in this case, however, good focus is evident in the resulting images due to the deviation being within the depth of field of the lens. The steep changes at the end of Fig. 10 show some blurring due to the deviation from the measured profile being larger than the depth of field.

5.2.3 Accuracy

Noise and deviations from a flat profile is seen in the measured height profile of the LEGO staircases used in the tracking (Fig. 10). This is due to specular reflections of the laser in the rather reflective surface of the LEGO (Fig. 12). This noise is in reality not prominent in the acquired across-track height profiles (Fig. 11), but are enhanced in the measured track profile due to the fact that it always chooses the maximum height of the profile. Even if the across-track profile has only one small reflection, it is picked up by the focus point selection algorithm.

Fig. 12 also shows a rather large laser line thickness, resulting in some uncertainty of the derived height profile. This can be adjusted by modifying both laser and camera parameters. For situations where the depth of field would be less than the accuracy of the current system, the self-developed laser triangulation system can also be exchanged by a more accurate, off-the-shelf laser measurement device. This sacrifices across-track modeling and dynamic focus point selection by a higher accuracy in the tracking. This approach has successfully been used in an earlier iteration of the autofocus system in the research group.

6. CONCLUSIONS AND FUTURE WORK

Camera focus is an important part of obtaining the necessary image quality for hyperspectral analysis. A complete system for focusing a push-broom hyperspectral camera has been developed. The system retains the focus during scan, and has been tested and found to perform well on various objects with different variations in the topography. The system is suitable for measurement applications in the lab, and for industrial applications that involve the imaging of objects on a conveyor belt. The system can obtain 3D models of the imaged objects. Further work will strive to take full advantage of the 3D models in rectifying challenging illumination conditions in the resulting images.

ACKNOWLEDGMENTS

Thanks to the HySpex group at Norsk Elektro Optikk AS for valuable discussions and collaboration in the integration of the autofocus system, and for manufacturing the autofocus calibration standard. Thanks to Terje Schjelderup for procurement of the LEGO staircases. The project is a part of the Iacobus project, `http://www.iacobus-fp7.eu`. Iacobus is supported by the European Commission's 7th RTD Framework Programme Collaborative Project No. 305760.

REFERENCES

[1] Keshava, N. and Mustard, J., "Spectral unmixing," *IEEE Signal Proc. Mag.* **19**, 44 –57 (jan 2002).
[2] Skauli, T., Haavardsholm, T. V., I., K., Arisholm, G., Kavara, A., Opsahl, T. O., and A., S., "An airborne real-time hyperspectral target detection system," *Proc. SPIE* **7695** (2010).
[3] Gowen, A. A., O'Donnell, C. P., Cullen, P. J., Downey, G., and Frias, J. M., "Hyperspectral imaging - an emerging process analytical tool for food quality and safety control," *Trends Food Sci. Tech.* **18**(12), 590–598 (2007).
[4] Tatzer, P., Wolf, M., and Panner, T., "Industrial application for inline material sorting using hyperspectral imaging in the nir range," *Real-time Imaging* **11**(2), 99–107 (2005).
[5] Randeberg, L. L., Larsen, E. L. P., and Svaasand, L. O., "Characterization of vascular structures and skin bruises using hyperspectral imaging, image analysis and diffusion theory," *J. Biophotonics* **3**(1-2), 53–65 (2010).
[6] Lu, G. and Fei, B., "Medical hyperspectral imaging: a review," *J. Biomed. Opt.* **19**(1), 010901 (2014).
[7] Sorg, B. S., Moeller, B. J., Donovan, O., Cao, Y., and Dewhirst, M. W., "Hyperspectral imaging of hemoglobin saturation in tumor microvasculature and tumor hypoxia development," *J. Biomed. Opt.* **10**(4) (2005).

[8] Randeberg, L. L. and Hernandez-Palacios, J., "Hyperspectral imaging of bruises in the swir spectral region," *Proc. SPIE* **8207** (2012).
[9] Paluchowski, L. A., Nordgaard, H. B., Bjorgan, A., Berget, S. A., and Randeberg, L. L., "Can spectral-spatial image segmentation be used to discriminate burn wounds?," *J. Biomed Opt.* (2016).
[10] Krotkov, E., "Focusing," *International Journal of Computer Vision* **1**(3), 223–237 (1988).
[11] Fontana, R., Barucci, M., Carcagni, P., Daffara, C., Pampaloni, E., and Pezzati, L., "Autofocus laser system for multi-nir scanning imaging of painting surfaces," *Proc. SPIE* **8084** (2011).
[12] Nasibov, H., Kholmatov, A., and Hacizade, F., "Investigation of autofocus algorithms for vis-nir and nir hyperspectral imaging microscopes," in [*NIR2013 Proceedings*], (2013).
[13] Subbarao, M. and Tyan, J.-K., "Selecting the optimal focus measure for autautofocus and depth-from-focus," *IEEE Trans. Pattern Anal. Machine Intell.* **20**(8), 864–870 (1998).
[14] Chen, C., Hwang, R., and Chen, Y., "Focusing techniques," *Appl. Soft Comput.* (2010).
[15] Kautsky, J., Flusser, J., Zitova, B., and Simberova, S., "A new wavelet-based measure of image focus," *Pattern Recogn. Lett.* **23**(14), 1785–1794 (2002).